Title

Periodic magnetic fieldas a polarized and focusing thermal neutron spectrometer and monochromator

Authors

Cremer, J T
D. L. Williams
M. J. Fuller
et al.

Publication Date

2010-01-12

Peer reviewed

Periodic magnetic field as a polarized and focusing thermal neutron spectrometer and monochromator

J. T. Cremer,[1,a] D. L. Williams,[1] M. J. Fuller,[1] C. K. Gary,[1] M. A. Piestrup,[1] R. H. Pantell,[2] J. Feinstein,[2] R. G. Flocchini,[3] M. Boussoufi,[3] H. P. Egbert,[3] M. D. Kloh,[3] and R. B. Walker[3]
[1]*Adelphi Technology, Inc., 2003 East Bayshore Rd., Redwood City, California 94063, USA*
[2]*Department of Electrical Engineering, Stanford University, Stanford, California 94305, USA*
[3]*Davis McClellan Nuclear Radiation Center, University of California, McClellan, California 95652, USA*

(Received 11 June 2009; accepted 23 November 2009; published online 12 January 2010)

A novel periodic magnetic field (PMF) optic is shown to act as a prism, lens, and polarizer for neutrons and particles with a magnetic dipole moment. The PMF has a two-dimensional field in the axial direction of neutron propagation. The PMF alternating magnetic field polarity provides strong gradients that cause separation of neutrons by wavelength axially and by spin state transversely. The spin-up neutrons exit the PMF with their magnetic spins aligned parallel to the PMF magnetic field, and are deflected upward and line focus at a fixed vertical height, proportional to the PMF period, at a downstream focal distance that increases with neutron energy. The PMF has no attenuation by absorption or scatter, as with material prisms or crystal monochromators. Embodiments of the PMF include neutron spectrometer or monochromator, and applications include neutron small angle scattering, crystallography, residual stress analysis, cross section measurements, and reflectometry. Presented are theory, experimental results, computer simulation, applications of the PMF, and comparison of its performance to Stern–Gerlach gradient devices and compound material and magnetic refractive prisms. © *2010 American Institute of Physics.* [doi:10.1063/1.3274512]

I. INTRODUCTION

Neutrons possess spin and an associated magnetic dipole moment, and the force exerted between the magnetic dipole moment and a magnetic field gradient may be used to control the neutron trajectory. By such means, a variety of neutron magnetic, optical elements can be fabricated, such as lenses,[1–14] mirrors,[14,15] field gradient devices,[14–16] and spin flippers,[15] as well as prisms.[2,5,6,8] Single or polycrystals, which filter by preferential scattering or absorption, thin film, multilayer metallic mirrors, field gradient devices such as the Stern–Gerlach polarimeter,[14–16] and multipole magnets, such as the sextupole[5] can produce polarized neutrons. Shimizu[5] focused and polarized cold neutrons (such as 14.4 Å) with a two-dimensional (2D) quadrupole magnetic lens, and with two different 2D sextupole magnetic lenses, a Halbach type permanent magnet sextupole with 25 mm bore diameter, and a superconducting sextupole magnet with 46.8 mm bore diameter.

Polarized neutrons have also been produced by refraction with magnetic fields in vacuum (or air) in the shape of prisms and cylindrical lenses. Just *et al.*[2] obtained prism shaped magnetic fields by taper cutting the cylindrical iron-core pieces of a split electromagnet into triangle-shaped pole pieces. The neutron deflection achieved by a single prism-shaped material or magnetic field is small and inadequate to spectrally disperse short wavelength neutron beams efficiently. However, a row of *N* identical prisms or lenses (material or magnetic), which forms, respectively, a compound refractive prism (CRP) or compound refractive lens (CRL) increases the deflection angle and dispersion[1–13] by *N*-fold. Littrell *et al.*[7] constructed and tested a one-dimensional (1D) magnetic compound refractive lens, which used a 99 pairs of cylindrical magnets to produce cylindrical-shaped magnetic fields in air, which focused and polarized cold neutrons (4–13 Å).

Recently, we investigated several magnet configurations and developed a novel design, a periodic magnetic field (PMF) neutron optic, which can focus and separate neutrons axially by wavelength and vertically by spin. The PMF is an arrangement of alternating north-south poles (Fig. 1), which forms a half-wiggler magnet configuration, similar to the full wigglers of synchrotron x-ray sources. Also, the relatively inexpensive PMF can provide strong, transverse, magnetic field gradients over relatively long axial lengths (2–3 m), which causes relatively large vertical neutron deflections and separation of spin states.

Spin-down neutrons in the PMF are deflected downward, unfocused toward the PMF pole faces. The spin-up neutrons (higher energy spin state) are deflected upward and are focused into horizontal lines at a fixed vertical distance in a parallel plane above the PMF surface plane, see Figs. 2 and 3. This vertical distance is proportional to the period of the PMF periodic magnetic field, but is independent of the neutron wavelength. The axial focal distance of the line-focused neutrons, which is measured from the PMF exit is proportional to the neutron energy, and inversely proportionally to the square of the neutron wavelength. The PMF magnetic

[a]Electronic mail: ted@adelphitech.com. Tel.: 650-474-2750 x 16. FAX: 650-474-2755.

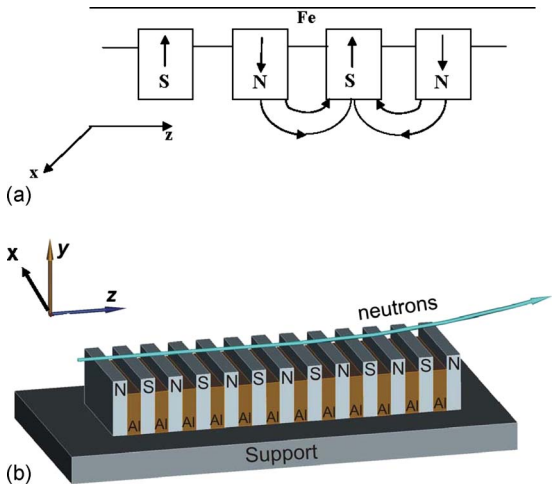

FIG. 1. (Color online) Shown in (a) is the profile of magnetic field lines of a single period of the PMF and (b) a schematic of the PMF with its alternating magnetic poles separated by aluminum spacers.

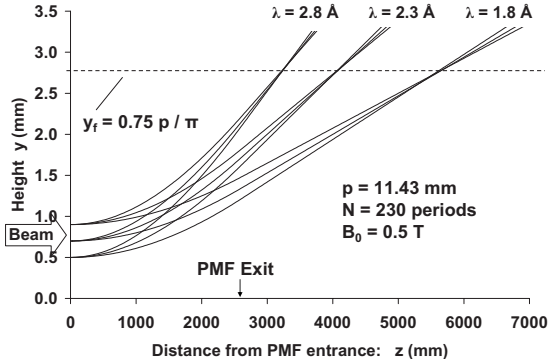

FIG. 3. Shown are trajectory plots for 1.8, 2.3, and 2.8 Å spin-up neutrons in a horizontal strip beam that pass through the PMF and line focus downstream of its exit. For each wavelength λ, neutrons with zero initial divergence angle are centered at initial height y_0=0.7 mm with lower and upper beam boundaries at y_0=0.5 and 0.9 mm. The force on spin-up neutrons in the PMF is unidirectional and decreases exponentially from its surface at y=0. Neutron paths closer to the PMF surface cross neutron paths that are further away in a fixed plane at critical height y_f=2.72 mm above the PMF surface (shown by horizontal dashed line). The PMF parameters are N =230 periods, period length p=11.43 mm, and surface magnetic field amplitude B_0=0.5 T. The spin-up neutrons transition from an upward curved trajectory, which is caused by the magnetic field gradient in the 2.63 m long PMF to a straight line trajectory extending from its exit through the field-free drift space to a linear detector.

field lines lie in vertical planes above the PMF surface and the spin-up neutrons exit the PMF with their longitudinal magnetic moments aligned antiparallel to the direction of the last encountered PMF magnetic field lines. Thus, a detector can scan along the axial direction at a fixed vertical distance above the pole faces to record the spectral distribution of the aligned (polarized) spin-up neutrons.

Possible applications of material and magnetic PMFs include monochromators and spectrometers, given a sufficiently strong neutron source. Combined with collimating slits, the PMF can act as a monochromator that provides a narrow bandwidth of neutrons to targets such as crystals for neutron diffraction (Fig. 2). As a spectrometer, a PMF presents the entire spectrum at once rather than having to scan through wavelengths such as a chopper or crystal. The focusing, dispersive, and polarizing properties of the PMF could make it useful in residual stress analysis, reflectometry, small angle neutron scattering, and neutron absorption measurements. Magnetic thin films, which allow the construction of recording and storage media, as well as sensors, can be analyzed using polarized neutrons of the PMF. The PMF can also be applied to beams of electrons, protons, and ions (e.g., ^{3}He) that have a magnetic dipole moment. In the general case of particles with dipole magnetic moments, the magnetic field gradient of the PMF transversely separates the up and down spin states and axially separates and line focuses the particles by their energy in a parallel plane above the PMF surface.

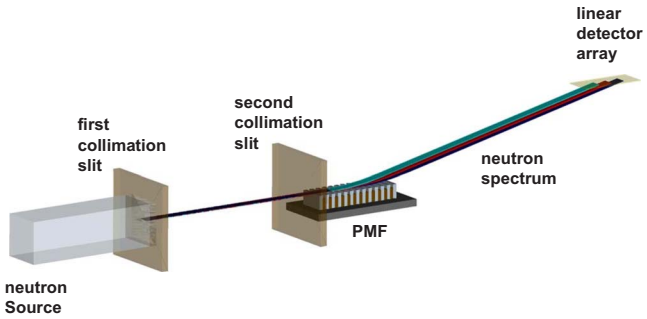

FIG. 2. (Color online) The PMF provides equal and opposite vertical deflection of neutron spin states and axial separation of neutron wavelengths. The higher energy state, spin-up neutrons ($\mu_\parallel$ aligned antiparallel to **B**) are deflected upward from PMF magnet surface. The pair of collimation slits reduces the initial neutron beam divergence to less than the deflection angle acquired by the neutrons in the PMF. The PMF provides 1D horizontal line focusing of neutrons along an axial line parallel and above the PMF surface in which the focal distance measured from the PMF exit increases proportionally with neutron energy.

II. THEORY

The PMF in Fig. 1 consists of an axial (z-axis) row of N rectangular magnets with alternating magnetic polarity in the vertical (y-axis) direction. Along the z-axis, the magnets of axial width Δz_m are separated by aluminum spacers of axial width Δz_s. Neutrons propagate in the axial z-direction through the sinusoidal magnetic field lines **B**, which lie in parallel, vertical yz-planes that intersect the horizontal xz-plane of the PMF surface. The magnets can be permanent, or alternatively can be continuous or pulsed electromagnetic magnets.

The PMF magnetic field component in the transverse x-direction is zero, but it varies periodically with spatial period p in the axial z-direction and vertical y-direction. The periodic PMF magnetic field along z is achieved by a line of magnets whose surface polarity alternates; N-S-N-S-N-S$\cdots$N-S, where the dash indicates the aluminum spacer between each pair of magnets. A single period p consists of two magnets with surface poles N and S, separated by an aluminum spacer and followed by another aluminum spacer. The magnetic field amplitude at the magnet surface is determined by the vertical magnetization vector **M** of the magnet, and in this case are rectangular, neodymium (NdFeB, grade 42), permanent magnets.

The PMF magnetic field is periodic in y and z, but decreases with vertical distance y, which is measured from the

$y=0$ horizontal plane of the PMF magnet surface. At the magnetic pole surfaces the magnetic field is directed vertically, and alternates downward $(-\hat{\mathbf{y}})$ or upward $(+\hat{\mathbf{y}})$. The PMF magnetic field $\mathbf{B}$ has an exponential amplitude $|\mathbf{B}|$, which decreases with increasing distance y from its maximum amplitude at the PMF magnet surface at $y=0$. The magnetic field $\mathbf{B}$ can be approximated by the simple analytic expression

$$\mathbf{B} = \left[\hat{\mathbf{y}}\cos\left(\frac{2\pi}{p}z\right) + \hat{\mathbf{z}}\sin\left(\frac{2\pi}{p}z\right)\right]Y(y). \quad (1)$$

The magnitude of the magnetic field $|\mathbf{B}|$ is magnetic field amplitude $Y(y)$ given by

$$|\mathbf{B}| = Y(y) = z_r B_0 \exp\left(-\frac{2\pi}{p}y\right). \quad (2)$$

The above magnetic field expression is a convenient and reasonable approximation of the PMF magnetic field because $\mathbf{B}$ has the periodicity of the PMF structure and $\mathbf{B}$ satisfies Maxwell's equations for the static case; namely, $\nabla\times\mathbf{B}=0$ and $\nabla\cdot\mathbf{B}=0$. In addition to the magnetization vector $\mathbf{M}$ of the individual magnets, the PMF magnetic field is dependent upon the Fourier coefficient z_r. That is, the PMF magnetic field $\mathbf{B}$ is modeled as the first harmonic of a magnetic field that has periodic reversal of polarity (bipolar pulse train) with surface magnetic field amplitude B_0 and period p in which $\mathbf{B}$ has Fourier coefficient z_r, amplitude $Y(y)$, and period p. The Fourier coefficient z_r is a function of the ratio of the magnet width divided by the spacer width, $\Delta z_m/\Delta z_s$. For equal magnet and aluminum spacer widths, $\Delta z_m=\Delta z_s$, the Fourier coefficient is $z_r=2\sqrt{2}/\pi$ or 0.90.

Assume the neutron is propagating in the positive axial z-direction, and enters the PMF at time $t=0$ and $z=0$, and at vertical position $y(0)=y_0$ above the PMF magnet surface with approximate constant axial velocity v_0. The neutron axial position z in the PMF is related to its elapsed passage time t at z by $z=v_0t$. As the neutron propagates axially through the PMF magnetic field, the neutron experiences a time varying magnetic field in its rest frame. Setting $z=v_0t$ in Eq. (1) yields the time-varying PMF magnetic field that is encountered by the neutron,

$$\mathbf{B}(t) = Y(y)\hat{\mathbf{b}}(t) = Y(y)[\hat{\mathbf{y}}\cos wt + \hat{\mathbf{z}}\sin wt]. \quad (3)$$

The temporal angular frequency w of oscillation in the y and z directions experienced by the neutron in the magnetic field is $w=2\pi v_0/p$. Given Planck's constant h and neutron mass m, the de Broglie relation $\lambda=h/mv_0$ between the neutron wavelength λ[Å] and momentum mv_0 yields the neutron velocity v_0[mm/s] in the z-direction where $v_0=3.96\times10^6/\lambda$. With period p[mm], the angular temporal frequency w[rad/s] of the PMF magnetic field that acts on the neutron rest frame is $w=2.49\times10^7/p\lambda$. Every half period $t_{1/2}=\pi/w$ or $t_{1/2}$[s]$=1.26\times10^{-7}$ $p\lambda$ the neutron encounters 180° reversal of magnetic field direction.

A magnetic potential energy $U=-\boldsymbol{\mu}\cdot\mathbf{B}$ is acquired by a neutron of magnetic moment $\boldsymbol{\mu}$ and spin angular momentum $\mathbf{I}$ in the applied PMF magnetic field $\mathbf{B}$. The neutron has a magnetic moment $\boldsymbol{\mu}$ that is antiparallel to its angular momentum $\hbar\mathbf{I}$, where $\hbar=h/2\pi$. The proportionality constant between $\boldsymbol{\mu}$ and $\mathbf{I}$, namely, the gyromagnetic ratio,[17–21] $\gamma=2g\mu_n/\hbar$, is negative, where $\boldsymbol{\mu}=\gamma\hbar\mathbf{I}$ or $\boldsymbol{\mu}=2g\mu_n\mathbf{I}$, because the Landé g factor is negative for the neutron, where $g=-1.91$. The nuclear dipole moment or magneton μ_n is expressed in SI units by $\mu_n=e\hbar/2m$ with neutron mass m and elementary charge e, where $\mu_n=3.15\times10^{-8}$ eV/T, and $\gamma=-1.83\times10^8$ in units of T^{-1} rad/s. The longitudinal or magnetic spin component $I_z=I\cos\chi$ of the spin angular momentum $\mathbf{I}$, which is parallel (+) or antiparallel (−) to magnetic field $\mathbf{B}$, has two allowed magnetic quantum numbers $I_z=\pm1/2$. With $|\mathbf{I}|=\sqrt{I(I+1)}$, $I=1/2$, and $I_z=\pm I$. Relative to the magnetic field vector $\mathbf{B}$ direction, the neutron spin vector $\mathbf{I}$ is oriented at polar (spin orientation) angle $\chi=\cos^{-1}(I_z/|\mathbf{I}|)$ or $\chi=54.7°$ for spin-up neutrons with I_z and $\mathbf{B}$ parallel, and $\chi=125.3°$ for spin-down neutrons with I_z and $\mathbf{B}$ antiparallel, where magnitude $|\boldsymbol{\mu}|=\mu=g\mu_n\sqrt{3}$ or $\mu=1.04\times10^{-7}$ eV/T.

The neutron magnetic dipole moment vector $\boldsymbol{\mu}$ is oriented at polar (magnetic moment orientation) angle θ relative to the magnetic field vector $\mathbf{B}$, and the neutron acquires potential energy $U=-\mu|\mathbf{B}|\cos\theta$, where $\theta=180°-\chi$. By convention,[20] the magnetic dipole moment vector $\boldsymbol{\mu}$ points from the magnetic south to north pole, and the magnetic field vector $\mathbf{B}$ points from the magnetic north to south pole. The longitudinal component of $\boldsymbol{\mu}$ is $\mu_\parallel=\mu\cos\theta$, and $\mu_\parallel$ is aligned parallel or antiparallel to the magnetic field direction $\mathbf{B}$, where in the case of $\boldsymbol{\mu}$ relative to $\mathbf{B}$, the magnetic moment orientation angle is $\theta=125.3°$ for spin-up neutrons and $\theta=54.7°$ for spin-down neutrons. Since $\boldsymbol{\mu}=2g\mu_n\mathbf{I}$, the longitudinal component of $\boldsymbol{\mu}$ becomes $\mu_\parallel=2g\mu_nI_z$ or $\mu_\parallel=\pm g\mu_n$, and the magnetic potential energy U[eV] acquired by the magnetic dipole in magnetic field B[T] is $U=-\mu_\parallel|\mathbf{B}|$, where $\mu_\parallel=\pm6.01\times10^{-8}$ eV/T for spin-down (+) and spin-up (−) neutrons. The spin-down neutrons are in the lower spin state with energy $U=-6.01\times10^{-8}|\mathbf{B}|$ in which $\mu_\parallel$ is aligned parallel to $\mathbf{B}$, and the spin-up neutrons are in the higher energy state $U=6.01\times10^{-8}|\mathbf{B}|$ with $\mu_\parallel$ aligned antiparallel to $\mathbf{B}$.

A neutron enters the PMF magnetic field $\mathbf{B}$, and its magnetic moment vector $\boldsymbol{\mu}$ begins azimuthal precession at the Larmor frequency $\Omega=\gamma B$ at polar orientation angle θ about the magnetic field direction, independent of its wavelength λ[Å]. The neutron's initial longitudinal magnetic moment $\mu_\parallel=\mu\cos\theta$ is either parallel or antiparallel to the direction of the magnetic field. A spin-up (spin-down) neutron maintains its longitudinal magnetic moment component $\mu_\parallel$ in a fixed antiparallel (parallel) alignment with respect to the periodically varying direction of the PMF magnetic field lines. Moreover, in so doing the neutron magnetic moment vector $\boldsymbol{\mu}$ is kept at a constant polar orientation angle θ (125.3° for spin-up and 54.7° for spin-down neutrons) with respect to the PMF magnetic field vector $\mathbf{B}$[T], provided the temporal variation of the magnetic field w is much less than the azimuthal Larmor precession frequency Ω, where $\Omega\gg w$. As the magnetic field with half period $t_{1/2}$ changes direction, the neutron realignment occurs within a Larmor precession period t_Ω[s]$=2\pi/\Omega$, provided $t_{1/2}/t_\Omega\gg1$, where $t_{1/2}/t_\Omega=3.67p\lambda B$ for PMF period p[mm].

At room temperature and 1–10 T magnetic fields the Boltzmann equation shows $\mu_\parallel$ is aligned with almost equal

probability parallel (0°) or antiparallel (180°) to the direction of the magnetic field, where $\mu=\sqrt{\mu_{\|}^2+\mu_{\perp}^2}$ and $\mu_{\|}$ are each constant, and with polar orientation angle θ, determines the remaining nonzero, transverse component, $\mu_{\perp}=\mu \sin\theta$, which is perpendicular to $\mathbf{B}$. The magnetic field $\mathbf{B}=\Omega\hat{\mathbf{b}}$ with unit vector $\hat{\mathbf{b}}$, varies in periodically in directions y and z as a function of PMF axial position z, or time of flight t, and the magnetic moment vector $\boldsymbol{\mu}$ has x, y, and z components (μ_x,μ_y,μ_z) that each vary periodically with position z or time t within the PMF.

The electromagnetic energy loss from neutron magnetic dipole precession in the PMF magnetic fields is zero.[22] Also, the neutron dipole-lattice T1 longitudinal energy decay with the PMF structure and the T2 dipole-dipole transverse dephasing decay between neutrons in the beam are assumed negligible.[17–19]

Interestingly, the Bloch equation $d\boldsymbol{\mu}/dt=\gamma\mathbf{B}\times\boldsymbol{\mu}$ solution for the magnetic moment vector $\boldsymbol{\mu}$ and the Lorentz force equation $d\mathbf{v}/dt=(e/m)\mathbf{v}\times\mathbf{B}$ solution for velocity vector $\mathbf{v}$ are identical, if one sets $e/m=-\gamma$ for particle mass m, charge e, and gyromagnetic ratio γ, which is proportional to the particle's Landé g factor. For example, the ratio e/m in the Lorentz force equation solution for the velocity vector $\mathbf{v}$ of a ^{3}He nucleus through the PMF magnetic field, can be replaced by minus the ^{3}He gyromagnetic ratio $(-\gamma)$ to obtain the PMF trajectory of the ^{3}He magnetic moment vector $\boldsymbol{\mu}$.

The force $\mathbf{F}$ acting on a neutron of mass m is $\mathbf{F}=-\nabla U$ or $\mathbf{F}=-\mu_{\|}\nabla|\mathbf{B}|$. The spin-up and spin-down neutrons are deflected in opposite directions. The force acting on the higher energy, spin-up neutrons, is $\mathbf{F}=-6.01\times10^{-8}\nabla|\mathbf{B}|$ and for the spin-down, lower energy neutrons, $\mathbf{F}=6.01\times10^{-8}\nabla|\mathbf{B}|$. The PMF magnetic field $\mathbf{B}$ decreases with increasing distance from its surface, so that $\nabla|\mathbf{B}|<0$, and thus the spin-up neutrons are deflected upward, and the spin-down neutrons are deflected downward. The adiabatic condition of constant θ between $\boldsymbol{\mu}$ and $\mathbf{B}$ causes the PMF magnetic gradient force on the neutron to be unidirectional in the y-direction, such that spin-up (spin-down) neutrons are deflected vertically upward (downward) as the neutron propagates through the PMF.

The force acting on the neutron is also expressed by Newton's second law, $\mathbf{F}=m\mathbf{a}$, and hence the neutron acceleration in the magnetic field gradient is $\mathbf{a}=-\alpha\nabla|\mathbf{B}|$ with mass trajectory constant $\alpha=\mu_{\|}/m$. Since $\alpha=\mu_{\|}c^2/mc^2$ and given neutron rest mass energy $mc^2=9.38\times10^8$ eV, one obtains α in units of $\mathrm{mm}^2/\mathrm{s}^2\,\mathrm{T}$, where $\alpha=5.77\times10^6$ for spin-up neutrons ($\mu_{\|}$ antiparallel $\mathbf{B}$), and $\alpha=-5.77\times10^6$ for spin-down neutrons ($\mu_{\|}$ parallel $\mathbf{B}$).

The neutron position $\mathbf{r}(t)$ as a function of time t in the PMF magnetic field $\mathbf{B}$ is determined from acceleration $\mathbf{a}=-\alpha\nabla|\mathbf{B}|$, where $\mathbf{a}=(d^2y/dt^2)\hat{\mathbf{y}}$ and vertical velocity component $v_T=dy/dt$. The spin-up neutron is assumed to enter the PMF entrance with initial vertical height $y(0)=y_0$ above the PMF surface and has zero initial vertical velocity, $v_T(0)=0$. The neutrons propagate along the z-axis and undergo deflection in the vertical y-direction by the magnetic field. Since $B=Y(y)$, and $dB/dy=(-2\pi/p)B$, one obtains

$$\frac{d^2y}{dt^2}=\pm2\pi\frac{z_rB_0\alpha}{p}\exp\left(-\frac{2\pi}{p}y\right). \tag{4}$$

The + sign applies to spin-up neutrons, and the − sign to spin-down neutrons. With equal magnet pole and gap widths, $\Delta z_m=\Delta z_s$, the PMF has Fourier coefficient $z_r=2\sqrt{2}/\pi$.

The spin-up neutron vertical deflection $y(t)$ is solved as follows. Equating $d^2y/dt^2=v_Tdv_T/dy$ with Eq. (4) yields $v_Tdv_T=A\exp(-2\pi\cdot y/p)dy$. Integration of both sides produces an expression for y as a function of v_T, $y(0)$, and $v_T(0)$. With $v_T=(dy/dv_T)(dv_T/dt)$, one solves for dv_T/dt and then integrates to obtain v_T[mm/s], which then yields the trajectory y[mm] of the spin-up neutron through the PMF. As a function of the neutron axial position z[mm] and PMF period p[mm] and surface magnetic field amplitude B_0[T], and assuming zero transverse neutron velocity at the PMF entrance, $v_T(0)=0$ with $z=v_0t$ and $v_0=dz/dt$, the spin-up neutron trajectory equations within the PMF are

$$v_T=\frac{dy}{dt}=\frac{dy}{dz}\frac{dz}{dt}=\frac{\mathrm{K}pv_0}{\pi}\tanh(\mathrm{K}z), \tag{5}$$

and

$$y=y_0+\frac{p}{\pi}\ln[\cosh(\mathrm{K}z)]. \tag{6}$$

The PMF spatial frequency constant $\mathrm{K}[\mathrm{mm}^{-1}]$ is

$$\mathrm{K}=\frac{\pi\sqrt{2z_rB_0\alpha}}{v_0p}\exp\left(-\frac{y_0\pi}{p}\right)=\frac{2.56\times10^{-3}\lambda\sqrt{B_0}}{p}\times\exp\left(-\frac{y_0\pi}{p}\right). \tag{7}$$

If the transverse neutron velocity at the PMF entrance is nonzero, $v_T(0)\neq0$, then with $c_2=\tanh^{-1}[v_T(0)/c_1]$ and $c_1=v_0\sqrt{(\mathrm{K}p/\pi)^2+(v_T(0)/v_0)^2}$, the spin-up neutron trajectory $y(z)$ within the PMF is more complicated, where

$$y=\frac{p}{2\pi}\ln\left[\frac{2z_rB_0\alpha}{c_1^2}\cosh^2\left(\frac{c_1\pi}{pv_0}z+c_2\right)\right]. \tag{8}$$

With zero transverse velocity at the PMF entrance, $v_T(0)=0$, one can obtain simplifying approximate expressions of the above spin-up neutron trajectory equations. The small argument approximation for the hyperbolic tangent and cosine are $\tanh u\cong u$ and $\cosh u\cong1$ for $u<0.4$ with 10% or better accuracy. If $\mathrm{K}z<0.4$, then as a function of position z[mm] within the PMF, the spin-up neutron vertical velocity and position simplify to $v_T(z)\cong\mathrm{K}^2pv_0z/\pi$ and $y(z)\cong y_0$. That is, if $\mathrm{K}z<0.4$, the spin-up neutron enters the PMF at $z=0$, and its vertical velocity v_T increases proportionally with axial transit distance z and $B_0\lambda/p$ within the PMF, but its vertical position $y(z)$ remains approximately constant.

To separate neutrons by wavelength and spin state, the PMF must impart larger deflection angles than the neutron beam divergence angles set by collimation. To create the largest beam deflection, the neutron beam should pass close to the PMF surface, where magnetic field gradients are largest. Collimation of the neutron beam just prior to the PMF is achieved by a pair of horizontal slits, each with vertical gap Δy_0 and separated by axial distance Z_s. At the first slit, which

is at distance L from the neutron source of diameter D, the neutrons have divergence angle $\theta_0 = D/L$. Sufficiently small Δy_0 and large Z_s further collimates the incident neutrons, reducing the range of their divergence angles to $\theta_d = \Delta y_0 / Z_s$ at the second slit, which is situated at the PMF entrance. The initial neutron divergence angle ϕ_0 is bounded by the beam divergence angle θ_d at the PMF entrance, where $-\theta_d \leq \phi_0 \leq \theta_d$. With sufficient collimation by the slit pair and with sufficient PMF magnetic field and number of periods, beam neutrons of sufficiently long wavelength then acquire deflection angles $\phi(l_1)$ at the PMF exit that exceed their initial range of divergence angles, where $\phi(l_1) > \theta_d$.

The deflection angle $\phi(z)$ and deflection angle axial gradient $d\phi/dz$ are important measures by which to compare the separation of neutron wavelengths and spin states by the PMF with other neutron optic devices. The deflection angle is the ratio of the z-dependent vertical spin-up neutron velocity $v_T(z)$, divided by its approximately constant axial velocity v_0, where $\phi(z) = v_T(z)/v_0$. Assuming zero initial deflection angle $\phi_0 = 0$ via $v_T(0) = 0$ at the PMF entrance, then at the PMF exit ($z = l_1$), spin-up neutrons enter the downstream drift space with upward deflection angle $\phi(l_1)$ given by

$$\phi(l_1) = \frac{v_T}{v_0} = \frac{\mathrm{K}p}{\pi}\tanh(\mathrm{K}l_1). \tag{9}$$

If $\mathrm{K}z \ll 1$ and with $N = l_1/p$, the deflection angle $\phi(l_1)$ of spin-up neutrons exiting the PMF is

$$\phi(l_1) = \frac{2\pi B_0 z_r l_1 \alpha}{p v_0^2}\exp\left(-2\pi\frac{y_0}{p}\right) = 2.08 \times 10^{-6} N \lambda^2 B_0 \exp\left(-2\pi\frac{y_0}{p}\right). \tag{10}$$

The axial gradient of the deflection angle $d\phi/dz$ of the PMF is the change in the neutron deflection angle per length of the PMF in which $d\phi/dz$ is dependent upon the PMF period p, where $p = l_1/N$. The PMF $d\phi/dz$ can be readily compared with those of other neutron deflection optics. For spin-up neutrons of wavelength λ propagating in the PMF ($0 \leq z \leq l_1$), the axial gradient $d\phi/dz$ of the deflection angle depends on the initial neutron vertical position y_0 at the PMF entrance, and the PMF period p and surface magnetic field amplitude B_0. For $\mathrm{K}z \ll 1$ and $v_T(0) = 0$, the axial gradient of the deflection angle along the length of the PMF is

$$\frac{d\phi}{dz} = \frac{2\pi B_0 z_r \alpha}{p v_0^2}\exp\left(-2\pi\frac{y_0}{p}\right) = 6.54 \times 10^{-6} B_0 \frac{N\lambda^2}{l_1 \pi} \times \exp\left(-2\pi\frac{y_0}{p}\right). \tag{11}$$

The π in the denominator is explicitly included to facilitate convenient comparison of the PMF $d\phi/dz$ with those of other neutron optics.

Neutron rays of wavelength λ, which enter the PMF entrance ($z = 0$) at initial vertical height y_0 that exceeds the critical height y_f above the PMF surface are not appreciably deflected by the PMF magnetic field gradient. Incident neutrons that enter the PMF below the critical height with $y_0 < y_f$ are deflected either vertically upward (spin-up) or downwards (spin-down) and acquire a vertical velocity component v_T. The spin-up neutron rays exit the PMF with terminal deflection angles $\phi(y_0, l_1)$ and propagate in a straight line trajectory through the downstream drift region to the detector or horizontal collection slit. The critical height y_f is defined as the height y above the PMF surface, where the magnetic field $\mathbf{B}$ and deflection angle axial gradient $d\phi/dz$ falls to about 22% of their values at the PMF surface, which sets $y_f = 0.75p/\pi$.

The focal length f is measured from the PMF exit at $z = l_1$. Spin-up neutrons of wavelength λ exit the PMF at height $y(l_1)$, travel upward in straight-line trajectories, and intercept a plane parallel to and at critical height $y_f = 0.75p/\pi$ above the PMF planar surface. This neutron trajectory line climbs vertical distance $\Delta y_f = y_f - y(l_1)$ in axial (focal) distance f. The trajectory line slope is defined by the PMF exit deflection angle $\tan\phi(l_1) \cong \phi(l_1)$ for $f \gg \Delta y_f$, where angle $\phi(l_1) = \Delta y_f / f$. A spin-up neutron with zero initial transverse velocity $v_T(0) = 0$ focuses at axial distance f[mm] downstream of the PMF exit where

$$f = \frac{y_f - y(l_1)}{\phi(l_1)} = \frac{1.23 \times 10^3 \exp\left(\frac{y_0\pi}{p}\right)}{\lambda\sqrt{B_0}\tanh(\mathrm{K}l_1)} \times \left[0.75\frac{p}{\pi} - \frac{p}{\pi}\ln[\cosh(\mathrm{K}l_1)] - y_0\right]. \tag{12}$$

With linear expansion of the exponential and the condition $\mathrm{K}l_1 < 0.4$, the focal length becomes

$$f = 1.53 \times 10^5 \frac{p}{\lambda^2 N B_0}\left[0.75 - \left(\pi\frac{y_0}{p}\right)^2\right]. \tag{13}$$

The expansion of the exponential for y_0 in Eq. (12) yields a constant term, which is the focal length, independent of the initial vertical height y_0 in the PMF. The expansion's quadratic and higher order terms in y_0 are responsible for the aberration in the PMF, and limits the sharpness of the PMF focus and its axial separation of wavelengths. From Eq. (13) a sharp focus is produced if $y_0\pi/p < 0.3$, and the focal length for spin-up neutrons is then approximated by

$$f = 1.1 \times 10^5 \frac{p}{\lambda^2 N B_0}. \tag{14}$$

The vertical height of the focal plane above the PMF surface $y_f = 0.75p/\pi$ for spin-up neutrons of wavelength λ can be increased by increasing the PMF period p, but to maintain the same focal length f with ratio $p/B_0 N$ unchanged, requires increasing by the same proportion the number of PMF periods N and/or the surface magnetic field amplitude B_0.

The spin-up neutron vertical height $y_d(z)$ upon exit from the PMF in the downstream drift space at distance z from the PMF entrance is

$$y_d = (z - l_1)\phi(l_1) + y(l_1). \tag{15}$$

At focal distance f downstream of the PMF exit ($z = l_1$), the center vertical height y_d of the horizontal line focus above the plane of the PMF surface is $y_d(f + l_1) = y_f$. The vertical width Δy_d about y_d[mm] depends on the initial neutron di-

vergence $|\phi_0| \leq \theta_d$. At distance z from the PMF entrance the vertical beam width is $\Delta y_d = z\theta_d$.

The vertical height trajectory $y(z)$ of a spin-up neutron, which enters the PMF with initial height y_0[mm] and zero slope [$\phi_0 = 0$ where $v_T(0) = 0$], is calculated as a function of axial transit distance z[mm] measured from the PMF entrance at $z=0$. The spin-up neutron vertical height $y(z)$ above the PMF surface within the PMF length ($0 \leq z \leq l_1$) is given by Eq. (6). Downstream of the PMF exit ($z \geq l_1$) and beyond to a sample, detector, or horizontal collection slit at distance z[mm] from the PMF entrance, via Eqs. (6), (9), and (15), the spin-up neutron vertical height $y(z)$ above the PMF surface is

$$y = y_0 + \frac{p}{\pi}\ln[\cosh(\mathrm{K}l_1)] + 8.14 \times 10^{-4}(z - l_1)\lambda\sqrt{B_0} \times \exp\left(-\pi\frac{y_0}{p}\right)\tanh(\mathrm{K}l_1). \quad (16)$$

The plots of Fig. 3 show PMF line-focusing of a strip neutron beam downstream of the PMF exit. The strip neutron beam is comprised of neutrons of three wavelengths $\boldsymbol{\lambda} = 1.8$, 2.3, and 2.8 Å. The strip beam is produced by the pair of collimation slits just upstream of the PMF entrance. For each wavelength, three spin-up neutrons with a zero initial y-velocity $v_T(0) = 0$, start from three different initial positions, $y_0 = 0.5$, 0.7, and 0.9 mm, which define the bottom, center and top of the strip beam. In Fig. 3 the PMF has $N = 230$ periods with equal pole and gap thickness ($z_r = 0.9$), and period $p = 11.43$ mm with an overall length $l_1 = 2629$ mm and surface magnetic field amplitude $B_0 = 0.5$ T. Spin-up neutrons are focused along a line parallel to the PMF surface at critical height $y_f = 2.73$ mm, shown by the dashed horizontal line in Fig. 3. The shorter wavelength 1.8 Å neutrons are line-focused further out at distance 5.5 m downstream of the PMF entrance, whereas neutrons of longest wavelength 2.8 Å focus in closer at 3.2 m. The spin-up neutrons transition from an upward curved trajectory, which is caused by the magnetic field gradient in the 2.63 m long PMF to a straight line trajectory extending from its exit through the field-free drift space to a linear detector.

The plots of Fig. 4 compare the vertical deflection angle ϕ of $\lambda = 1.8$ Å spin-up neutrons as the PMF length l_1 and the number of periods N is increased. Under the conditions of a fixed surface magnetic field amplitude $B_0 = 0.5$ T, the neutron vertical deflection angle ϕ[mrad] is plotted as a function of PMF length l_1[mm] for four PMF periods of 2, 5, 10, and 15 mm. The neutrons enter a PMF with zero initial vertical velocity $v_T(0) = 0$ at height $y(0) = 0.5$ mm above the PMF surface. For PMF lengths l_1 less than 4.0 m, the maximum deflection angle ϕ is approximately 0.8 mrad, which means the intrinsic angular spread of the beam would have to be significantly less than this value for the PMF to be effective. As seen from Fig. 4, the longer PMF periods p provide larger neutron vertical deflection, but the spin-up neutrons are then focused at larger axial distances downstream of the PMF entrance. After a sufficient PMF length l_1 and number of periods $N = l_1/p$, the neutron deflection angles ϕ reach their maximum value.

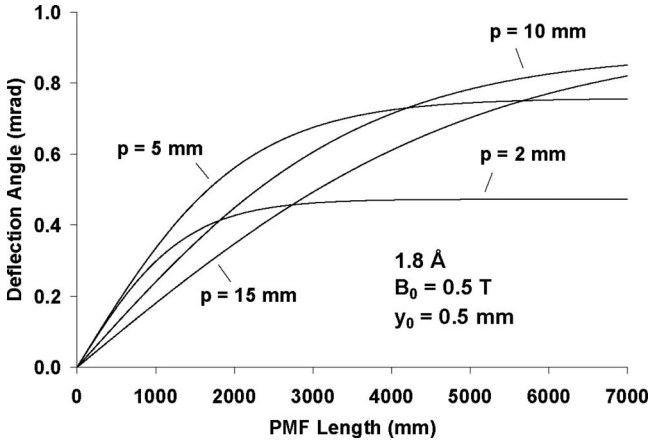

FIG. 4. The plots compare the vertical deflection angle ϕ of $\lambda = 1.8$ Å spin-up neutrons with increasing PMF length l_1 when the PMF period p is varied. As the PMF length l_1 increases, the number of periods N of length p increases as $N = l_1/p$. Fixed are the neutron initial height $y_0 = 0.5$ mm, zero transverse velocity $v_T(0) = 0$, and surface magnetic field amplitude $B_0 = 0.5$ T. Plotted are the deflection angle ϕ[mrad] curves for four PMF periods, $p = 2$, 5, 10, and 15 mm for increasing PMF length l_1[mm] and number of periods N.

III. EXPERIMENT

The PMF was tested for its ability to refract, deflect, and separate neutrons vertically by spin state and axially by wavelength at the thermal neutron beam line (bay 4) at the McClellan Nuclear Radiation Center (MNRC) reactor. The bay 4 beam line emerges from an underground reactor core at a 20° angle relative to the horizontal floor of bay 4. The Maxwell–Boltzmann distributed thermal neutrons pass from the reactor water core into the bay 4 beam tube through a graphite (moderator) end plug, and then pass through a 28 cm long sapphire crystal, which improves the thermal content by reducing the relative number of higher energy neutrons and gammas.

From the sapphire crystal the neutrons emerge from a 3.2 cm square source aperture in a boron carbide shielding plate, and propagate 3.0 m through a collimation tube to a horizontal slit, which is mounted on the aluminum face plate of the beam tube. The beam tube has scraper structures along its walls that aid in the removal of divergent neutrons and suppresses neutron scatter. The first horizontal slit, which is set on the aluminum face plate, has horizontal width 9.5 mm and vertical height 0.5 mm, and beyond this first slit is a massive sliding concrete door that opens to provide neutron exposure into bay 4.

In bay 4, mounted at the base of a Thor Laboratories 2.5 m long optical rail, is a second horizontal slit, which has horizontal width 9.5 mm and vertical height 0.4 mm. The second slit is 1.5 m downstream of the first slit, and the PMF is mounted on the rail immediately after the second slit [see Fig. 5(a)]. The rail is tilted at 20° relative to the floor to be aligned parallel with the neutron beam. The two collimation slits are aligned with the PMF via a laser, which is mounted on the downstream beam-stop wall. This wall laser provides a straight line laser beam, parallel to the neutron beam, between the center of the neutron source aperture and the neutron imaging detector [see Fig. 5(b)]. The small, square source aperture with side dimension $D = 31.75$ mm, and the

(a)

(b)

FIG. 5. (Color online) (a) Shown is front end of the 2.63 m long, 230 period, and 460 magnet pole PMF with the second collimation slit at its entrance. Each magnet is 3.175 mm in axial width and is separated by 2.54 mm axial width aluminum spacers. Each magnet period of $p=11.43$ mm is comprised of two magnets and two aluminum spacers set in the following order: N-surface pole magnet, aluminum spacer, S-surface pole magnet, and aluminum spacer. (b) Shown is the MNRC bay 4 beam line with the PMF in the foreground and in the background is the 20° inclined Bosch table on which is mounted the Fuji-film imaging plate.

long length of flight $L=10^4$ mm from the neutron source aperture to detector, produce collimation $L/D=315$ without the slits, which corresponds to divergence angle $\theta_{\mathrm{div}}=D/L$ or $\theta_{\mathrm{div}}=3.2\times10^{-3}$ rad.

The two collimation slits are needed to reduce the neutron beam's vertical divergence angle to less than the PMF deflection angle. The two slits have an average vertical height of 0.45 mm and are separated by 1.5 m, and thus the two slits reduce the neutron vertical divergence angle by a factor of ten to $\theta_d=3.0\times10^{-4}$ rad at the PMF entrance, where the neutron flux is 1.3×10^6 n cm^{-2} s^{-1} for neutron energies below 0.1 eV. The collimated neutron beam passes through the PMF and drift space to the downstream Fuji-film[23] neutron imaging plate or IP.

The Fuji-film IP is used to provide alignment and imaging. For initial alignment of the two collimation slits with the PMF, the IP is initially mounted at the end of the PMF. For final alignment the IP is set near the beam-stop wall, which is situated at maximum distance 5.64 m downstream from the second slit at the PMF entrance. For imaging the IP is mounted on a precision Bosch movable detector platform that is tilted 20° to match the bay 4 beam line. The detector can thus be translated toward the PMF, and scan the line-focused, spin-up neutrons whose energy decreases as the detector approaches the PMF.

The FCR XG-1NDT Fuji-film neutron imaging system uses an integrating position sensitive detector with high 18.2% quantum efficiency, 50 μm pixels, and five orders of dynamic range, and is based on the effect of photostimulated luminescence. One can obtain large area (23×25 cm^2) static, single shot images with the Fuji-film IP. The software package, DYNAMIX IMAGE SHARE VIEWER,[23] was used to display the Fuji-film neutron images.

We constructed and tested a 230-period PMF of length 2.63 m using 460 magnets (see Fig. 5), each magnet with a 3.175 mm axial width, and separated by 2.54 mm Al spacers. Two magnets, each magnet flanked by two spacers, comprised the magnet period of 11.43 mm in the axial direction of the neutron beam propagation. The NdFeB, grade 42 magnets had dimensions $12.7\times3.175\times12.7$ mm^3 with the magnetization along the 12.7 mm vertical dimension, and the field B_0 at the 3.175×12.7 mm^2 magnet surface was 0.45 T with maximum residual magnetic field B_r[T]=1.32, and BH_{max}[MG Oe]=42. The inexpensive magnets (0.89 USD per magnet) were acquired from K&J Magnetics (product No. B828). The aluminum spacers had dimensions $12.7\times2.54\times12.7$ mm^3, and the 2.54 mm axial width of the aluminum spacer was slightly smaller than that of the 3.175 mm magnet axial width so as to maximize the vertical magnetic field B_y.

The Fuji-film IP that imaged the neutrons was mounted 5.64 m from the PMF entrance and 3.01 m from the PMF exit. Following a 5 h exposure in this configuration, the IP was developed and the resulting image file was analyzed to determine the beam intensity profiles. The neutron beam produced an image at the IP with horizontal width 50 mm and vertical height 3 mm. The region of interest surrounding the neutron beam in the image had horizontal width in the x-direction of 78.6 mm and vertical height in the y-direction of 25.5 mm. This region of interest was divided into vertical strips of horizontal width 2.5 mm and vertical height 78.6 mm. The average value across the 2.5 mm horizontal width of the strip was determined at each height.

The plots in Fig. 6 show the measured, relative neutron intensity profile in the vertical (y) direction as a function of horizontal (x) position at the Fuji-film detector set 5.64 m from PMF entrance for a 5 h exposure. Figure 6(a) shows the unperturbed beam. It was measured from a region to the (left) side of the PMF at a horizontal (x) position of 25 mm, where the neutron beam was not significantly distorted by the magnetic field. Figures 6(b) and 6(c) show the splitting of the neutron beam in the presence of the PMF field at horizontal (x) positions of 32.5 and 42.5 mm, respectively. The direction of the splitting was in the y-direction. To a good approximation, the background intensity was observed to be linearly dependent upon y. This enabled background subtraction by assuming a straight line fit to intensity across the y-direction of the field of view. Following background subtraction, the best fit with two Gaussian distributions was calculated. Figure 6(d) shows the vertical (y) position of the peaks as a function of the horizontal (x) position where the scan was taken, which clearly indicates the neutron beam breaks into two components. The top component of the beam, corresponding to spin-up neutrons, is deflected upwards by 1.2 mm and the lower component of the beam, corresponding to spin-down neutrons, is deflected downwards by 0.8 mm relative to the center position of the non-deflected high energy neutrons.

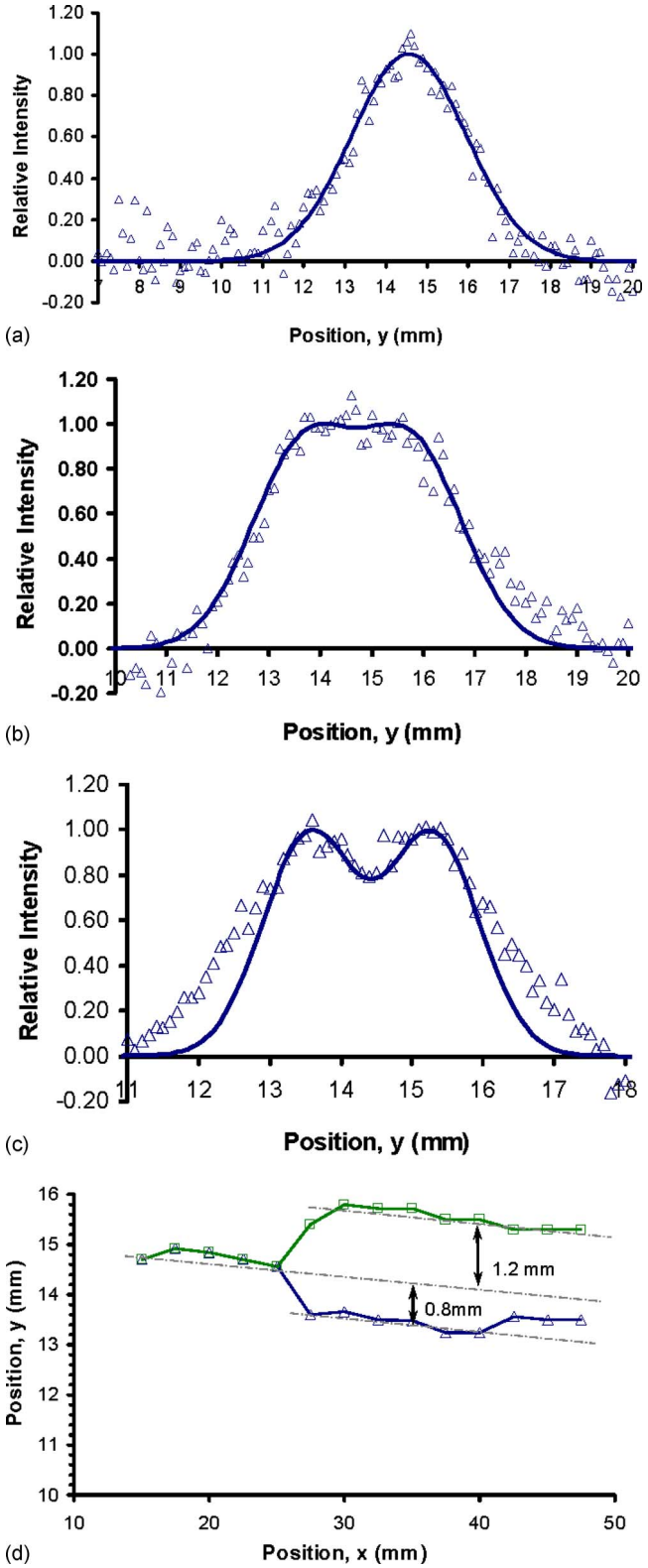

FIG. 6. (Color online) Shown is the measured data at the Fuji-film detector set 5.64 m from PMF entrance for 5 h exposure. (a) Plotted is the measured unperturbed neutron relative intensity profile in the vertical (y) direction at horizontal (x) position 25 mm from the left side of the detector image. In this position the neutron beam was relatively unperturbed by the PMF magnetic field. (b) Measured neutron relative intensity profile along y shows initial splitting of the neutron beam in the presence of the PMF field at horizontal (x) distance 32.5 mm from the left side. (c) Measured vertical (y) neutron relative intensity profile at horizontal (x) position 42.5 mm from the left side shows the vertical splitting of the neutron beam into two peaks at 13.5 and 15.3 mm. (d) Plotted is the vertical (y) position of the peaks as a function of the horizontal (x) position.

TABLE I. Computer simulation of PMF experiment.

Magnetic field amplitude at the pole surface	0.5 T
PMF period	11.43 mm
Number of PMF periods	230
PMF length	2629 mm
NdFeB magnet pole dimension (axial width)	3.175 mm
Aluminum spacer width between poles (axial width)	2.540 mm
PMF entrance to detector distance	5639 mm
PMF exit to detector distance	3010 mm
Full width beam divergence angle at the PMF entrance	0.30 mrad
Vertical height of beam center at PMF entrance	0.70 mm
Vertical beam width about beam center at PMF entrance	0.38 mm
Vertical beam width about beam center at detector	1.69 mm

A. Computer simulation and comparison with experiment

The above experiment demonstrated the splitting of a neutron beam into two beams, an upper spin-up beam and a lower spin-down beam by the periodic varying magnetic field of the PMF. A computer simulation of this experiment was performed and the computer simulation parameters are listed in Table I. The image intensity recorded on a detector may be calculated by ray tracing, as determined from the above derived neutron trajectory equations. This must be performed over the range of initial neutron transverse velocities and positions and wavelengths. It is assumed that the distributions for velocity and position are uniform, since slits were used to select a small fraction of the neutrons from the source.

The simulation characterized the flux distribution $\Phi(\lambda)$ of the neutron beam incident at the PMF as a wavelength dependent Maxwell–Boltzmann distribution, which is derived as follows. The Maxwell–Boltzmann neutron density distribution[24] for neutron velocities between v and $v+dv$ is $n(v)=Cv^2\exp(-v_r^2)$, where $v_r=v/v_t$ and $C=4n_0/v_t^3\sqrt{\pi}$, given the total neutron density n_0, and the neutron velocity $v_t=\sqrt{2kT/m}$ or corresponding de Broglie wavelength $\lambda_t=h/\sqrt{2mkT}$ at the distribution peak. For a beam of neutrons emerging from the reactor, the neutron flux spectrum as a function of velocity is $\Phi(v)=nv$, where $\Phi(v)dv=\Phi(\lambda)d\lambda$. From the de Broglie relationship $v=h/m\lambda$ and $dv=-hd\lambda/m\lambda^2$, the flux for neutrons with wavelengths between λ and $\lambda+d\lambda$ is then $\Phi(\lambda)\propto\lambda_0^5\exp(-\lambda_0^2)$, where $\lambda_0=\lambda_t/\lambda$. The peak neutron flux $\Phi_p(\lambda)$ occurs at wavelength $\lambda=\lambda_p$, where $\lambda_p=\lambda_t\sqrt{2/5}$, which MNRC estimates is $\lambda_p=1.1$ Å. The flux distribution $\Phi(\lambda)$ is normalized to unity at peak wavelength $\lambda_p=h/\sqrt{5mkT}$, so the relative neutron flux distribution $\Phi(\lambda)$ is then

$$\Phi(\lambda)=\left(\frac{\lambda_p}{\lambda}\right)^5\exp\left[2.5\left(1-\frac{\lambda_p^2}{\lambda^2}\right)\right]. \quad (17)$$

Plotted in Fig. 7 are the simulated and measured (5 h exposure), relative neutron intensities for the two neutron spin states with the Fuji-film detector set 5.64 m downstream of the PMF entrance. Assuming neutrons that strike the pole faces are not recorded by the detector, the calculated, relative image intensities on the detector for the two polarizations are indicated in Fig. 7(a). The $\Delta y_0=0.38$ mm width of incident

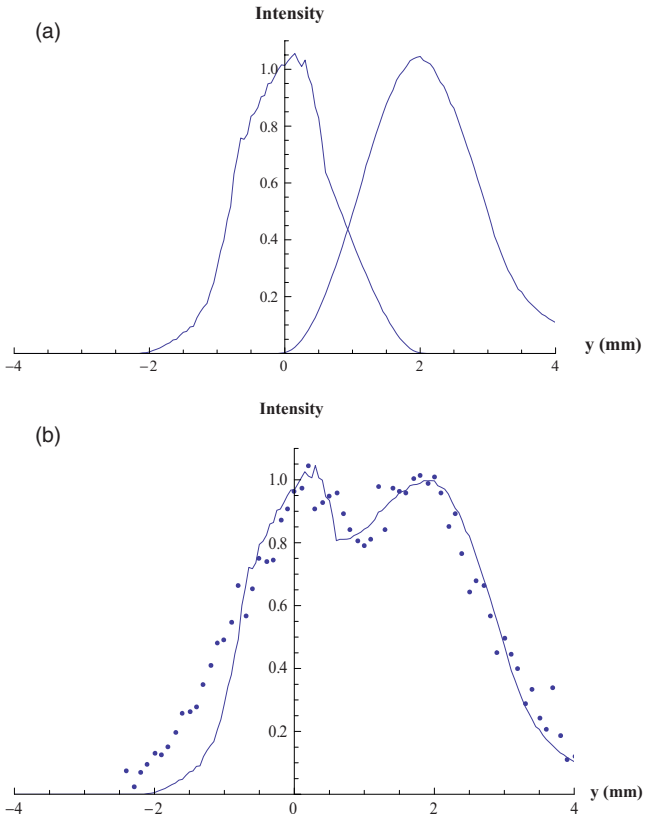

FIG. 7. (Color online) (a) Plotted are the calculated, relative intensities of neutrons at the detector for the two neutron spin states, which assume neutrons striking the PMF pole faces are not recorded on the detector, which is set 5.64 m downstream of the PMF entrance. (b) Plotted is the sum of the two calculated neutron spin spectra, which are displayed with the superimposed, measured PMF relative intensity spectrum that was obtained in a 5 h exposure with the Fuji-film detector.

neutron beam was centered at $y_0=0.7$ mm height above the PMF surface at its entrance, and the initial beam divergence set by the pair of upstream collimations slits was $\theta_d=0.3$ mrad. The divergence of the neutron beam caused it to expand to a vertical width of 1.69 mm at the detector. A collection slit, appropriately located in the detector plane, could transmit primarily one spin state or the other with excellent discrimination.

Shown in Fig. 7(b) is the experimental relative intensity data superimposed on the summed spectra of Fig. 7(a). The simulation falls below the data points on the left side of Fig. 7(b), which corresponds to neutrons that are directed toward the pole faces. In the simulation, neutrons that crossed the $y=0$ plane were not counted, but perhaps some of these penetrating neutrons reached the detector, which might explain the discrepancy between simulation and measurement.

B. Comparison of PMF with other neutron optics

The spatial separation of neutrons by wavelength and spin by the PMF is compared to other neutron optics. In particular the PMF is compared to the Stern–Gerlach field gradient device,[15,16] the compound material refractive prism,[5,6,8,14] and the compound magnetic refractive prism.[2,14]

First consider the Stern–Gerlach field gradient device, which has surface magnetic field B_g and gap d between its magnetic pole pair. A spin-up neutron, with approximately constant z-directed (axial) velocity v_0, experiences vertical y-directed acceleration a_y during its transit time $t=z/v_0$ through the field gradient device of length l_g, where $a_y=F_y/m$ and $F_y=-\mu_\parallel(dB/dy)$. At the gradient device exit $z=l_g$, a spin-up neutron has acquired transverse upward velocity $v_y=a_yt$ or $v_y=a_yz/v_0$. The neutron deflection angle is $\phi_g=v_y/v_0$ or $\phi_g=a_yz/v_0^2$, and its deflection angle gradient is $d\phi_g/dz=a_y/v_0^2$. With the vertical magnetic field gradient $dB/dy=B_g/d$ and $\alpha=\mu_\parallel/m$, the deflection angle ϕ_g at the gradient device exit $z=l_g$ is

$$\phi_g = l_g\frac{\alpha}{v_0^2}\frac{B_g}{d}. \tag{18}$$

The gradient device deflection angle gradient $d\phi_g/dz=\phi_g/l_g$ is independent of z. The ratio q_g of the neutron deflection angle $\phi(l_1)$ at the exit of a N-period PMF of length l_1 [Eq. (10)] with $y_0=0$ and $B_p=z_rB_0$, divided by the deflection angle ϕ_g of the gradient device of length l_g [Eq. (18)] is

$$q_g = 2\pi\frac{B_p}{B_g}\frac{d}{p}\frac{l_1}{l_g}. \tag{19}$$

In our experiments, with PMF period $p=11.43$ mm, length $l_1=2.63$ m, and surface magnetic field $B_p=0.45$ T, the PMF magnetic field to period ratio was $B_p/p=0.04$ T/mm, where $B_p=z_rB_0$ with $z_r=0.9$ and $B_0=0.5$ T. The PMF was 2.6 times longer ($l_1/l_g=2.6$), but its magnetic field to period ratio B_p/p was four times smaller than the magnetic field gradient B_g/d range of 0.15–0.10 T/mm of the Jones and Williams[16] Stern–Gerlach polarimeter. Based on these parameters at the device exit, the PMF produced a fourfold ($q_g=4.08$) larger deflection angle ϕ than the polarimeter, and independent of device length the PMF provided a 60% larger vertical deflection angle gradient $d\phi/dz$. In the future, larger PMF magnetic field gradients can be created by a current-carrying (pulsed or dc), serpentine ribbon conductor (normal or superconductor) similar to the Drabkin wiggler neutron spin flipper.[15]

The PMF performance is now compared with that of material and magnetic CRPs. A neutron with kinetic energy W_0 and mass m propagates in a material or vacuum magnetic field region and acquires potential energy U. In the neutron trajectory from source through the region of material or magnetic field to the detector, the total neutron energy E remains constant, and equal to the sum of its kinetic W and potential U energies. Hence, the neutron kinetic energy W_p in region with the material or vacuum magnetic field is less than its kinetic energy W_0 outside in a no-field vacuum; i.e., $W_p<W_0$, due to its acquisition of potential energy U. Using the de Broglie relation between neutron momentum h/λ and wavelength λ, the conservation of energy yields[1,3,14]

$$E=\frac{1}{2m}\left(\frac{h}{\lambda_m}\right)^2+U=\frac{1}{2m}\left(\frac{h}{\lambda}\right)^2. \tag{20}$$

The neutron wavelength λ_m in the material or magnetic field region is longer than its wavelength λ[Å] in the no-field vacuum. In the region with material or vacuum magnetic field, the refractive index is $n=\lambda/\lambda_m$, and solving for λ/λ_m yields $n^2=1-(U/E)$. The neutron kinetic energy exceeds its relatively weak potential energy, where $U\ll E$, so that the

refractive index is $n=1-\delta$ with dimensionless decrement $\delta=U/2E$. Since $E=W_0=W_p+U$, then $\delta=U/2W_0$ for neutron kinetic energy $W_0[\mathrm{eV}]=0.082/\lambda^2$ and the refractive index decrement δ becomes $\delta=mU(\lambda/h)^2$ or $\delta=6.1\lambda^2U$.

The effective force imposed on the neutron of wavelength λ by the potential energy gradient ∇U of the refractive medium is $\mathbf{F}=-\nabla U$ or $\mathbf{F}=-\nabla\delta/6.1\lambda^2$. For mediums comprised of magnetized or nonmagnetized materials or of applied magnetic fields, a nonuniform medium, such as a gradient index lens or a mirage in visible light optics, or more traditionally, the interface between two uniform media, produces a decrement gradient $\nabla\delta$ from which arises a wavelength dependent, deflection force $\mathbf{F}$ that refracts the passing neutrons. For example, a region of gravity has decrement $\delta_g=6.1\lambda^2mgy$ and decrement gradient $\nabla\delta_g=6.1\lambda^2\ mg\hat{\mathbf{y}}$, where the gravity force $\mathbf{F}_g=-mg\hat{\mathbf{y}}$ causes the vertical, downward deflection of a neutron with zero initial vertical velocity from its initial height y_0 as it propagates horizontally along z[mm].[3,4] This leads to a neutron vertical trajectory y[mm] $=y_0-3.12\times10^{-10}z^2\lambda^2$ via the gravitational field (acceleration) $\mathbf{g}[\mathrm{mm/s^2}]=9800$ and potential energy $U_g[\mathrm{eV}]=mgy$, so that the neutron deflection angle is $\phi[\mathrm{rad}]=\tan(y/z)$, and with $y\ll z$, its deflection angle axial gradient is $d\phi/dz[\mathrm{rad/mm}]=-3.12\times10^{-10}\lambda^2$.

In a material prism comprised of Q isotopes, each jth isotope with nuclei number density $\rho_j[\#/\mathrm{m^3}]$ and nuclei bound coherent scattering length $b_j[\mathrm{m}]$, bestows potential energy $U_j=\eta\rho_jb_j$ upon the neutron of mass m, where $\eta=h^2/2\pi m$, and the total nuclear potential energy acquired by the neutron is $U=\Sigma_{j=1}^{Q}U_j$. Hence, the decrement δ for materials is[14]

$$\delta=6.1\lambda^2\sum_{j=1}^{Q}\frac{\rho_jb_j}{2\pi}. \tag{21}$$

A prism comprised of fully magnetized ferromagnetic material is birefringent to neutrons, and uses scattering length b_j^F in place of b_j in Eq. (21). The bound coherent scattering length of each ferromagnetic isotope b_j^F is the sum[14] of its material bound coherent scattering length b_j and its magnetic scattering length b_j^M, where $b_j^F=b_j\pm b_j^M$ for neutrons with magnetic spin I_z parallel (+) or antiparallel (−) to $\mathbf{M}$. The magnetization vector $\mathbf{M}$ for a material of volume V is the volume-averaged magnetic moment $\boldsymbol{\mu}_i$ of the ferromagnetic nuclei in the material, where $\mathbf{M}=\Sigma_i\boldsymbol{\mu}_i/V$ in which $\mathbf{M}$ like $\boldsymbol{\mu}_i$ points from magnetic south to north, opposite that of an applied magnetic field $\mathbf{B}$. A fully magnetized iron prism has $b=9.54\ fm$ and $b^M=5.98\ fm$, and that of cobalt has $b=2.50\ fm$ and $b^M=4.64\ fm$.[14]

In mks units the Lorentz force equation $\mathbf{F}=q(\mathbf{v}\times\mathbf{B})$ defines the Tesla unit as $T=\mathrm{NA^{-1}\ m^{-1}}$, and the magnetic field $\mathbf{B}$[T] is proportional to the sum of the magnetizing or auxiliary field $\mathbf{H}$[A/m] (arising from free currents) and the magnetization $\mathbf{M}$[A/m] (arising from material bound currents) via the permeability constant for free space $\mu_0=4\pi\times10^{-7}\ \mathrm{N/A^2}$, where $\mathbf{B}=\mu_0(\mathbf{H}+\mathbf{M})$. Propagation through a fully magnetized ferromagnetic prism with magnetization $\mathbf{M}$ parallel to the prism faces, a neutron acquires potential energy $U_M=-\mu_0\boldsymbol{\mu}\cdot\mathbf{M}$ or $U_M=-\mu_\parallel\mu_0|\mathbf{M}|$ and experiences force $\mathbf{F}_M=-\nabla U_M$ or $\mathbf{F}_M=-\mu_\parallel\mu_0\nabla|\mathbf{M}|$, where $\mu_\parallel=\pm6.01\times10^{-8}$ eV/T. The lower energy state, spin-down (+) neutrons have moment $\mu_\parallel$ antiparallel and spin I_z parallel to $\mathbf{M}$, and the upper energy, spin-up (−) neutrons have $\mu_\parallel$ parallel and I_z antiparallel to $\mathbf{M}$. The material gradient (nuclear force) at the prism surfaces acts to equally deflect the spin-down and spin-up neutrons in an upward direction away from the prism base, whereas the magnetization gradient at the prism surfaces acts to deflect the lower energy state, spin-down neutrons upward ($b_j^F=b_j+b_j^M$) and the spin-up neutrons downward ($b_j^F=b_j-b_j^M$), while the prism magnetization can cause neutron spin flipping and depolarization of polarized neutron beams.[15]

An applied magnetic field $\mathbf{B}$ in vacuum (or air), which is shaped into a prism, creates a refractive medium with decrement $\delta=6.1\lambda^2U$ and a neutron of magnetic moment $\boldsymbol{\mu}$ and spin angular momentum $\mathbf{I}$ acquires potential energy $U_B=-\mu_\parallel|\mathbf{B}|$ and experiences force $\mathbf{F}_B=\mu_\parallel\nabla|\mathbf{B}|$ so that $\delta=-6.1\lambda^2\mu_\parallel|\mathbf{B}|$, where $\mu_\parallel=\pm6.01\times10^{-8}$ eV/T. The lower energy state, spin-down (+) neutrons have moment $\mu_\parallel$ parallel and spin I_z antiparallel to $\mathbf{B}$, and the upper energy, spin-up (−) neutrons have $\mu_\parallel$ antiparallel and spin I_z parallel to $\mathbf{B}$. For 1.8 Å neutrons, a 1.0 T magnetic field produces magnetic field decrement $\delta\cong1.18\times10^{-6}$, similar in magnitude to the material decrement of aluminum $\delta\cong1.07\times10^{-6}$.

A PMF with N periods is now compared with a material or magnetic CRP of the same length l_1, which is comprised of N material or magnetic prisms with $2N$ prism-air interfaces. Each material or magnetic prism has an apex angle α. The material prisms are created by fabricating a sawtooth pattern in a rectangular bar of material or by stacking material prisms in one or more rows.[5,6] In the magnetic prism the prism-shaped magnetic field is produced by a pair triangular magnetic pole pieces,[2,14] which are separated by a gap that are small compared with the pole surface dimensions.

A neutron ray is refracted at each material or magnetic prism surface by angle $\Delta\theta$ from angle θ_1 to θ_2 with respect to the prism surface normal, where $\theta_2=\theta_1+\Delta\theta$ and $\Delta\theta\ll1$. Snell's law gives $\sin\theta_1=(1-\delta)\sin(\theta_1+\Delta\theta)$ and $(1-\delta)\sin\theta_1=\sin(\theta_1+\Delta\theta)$ at the left and right prism surfaces. Each surface causes ray angular deviation $\Delta\theta=\delta\tan\theta_1$ in the same direction via the sine angle sum identity. The prism is an isosceles triangle with apex half-angle $\alpha/2$ and height h with base half-width $w=h\tan(\alpha/2)$. The slopes of the left (+) and right (−) prism surfaces relative to the base are $dh/dw=\pm\cot(\alpha/2)$, and hence, the surface normal slopes are $-dw/dh$. The incident ray is assumed parallel to the prism base, where $\theta_1=\alpha/2$, and so the slopes of the left (−) and right (+) surface normal are also $\pm\tan\theta_1$, and hence the deflection angle at each prism surface is $\Delta\theta=\delta\tan(\alpha/2)$.

Due to the very small deflection angle $\Delta\theta$ by each prism (because $\delta\ll1$), the neutron ray is nearly parallel to the prism bases in its passage through a N-prism CRP, so the total CRP deflection angle is approximated by $\theta_p=2N\Delta\theta$. Each prism[2,14] deflects an incident ray by angle $2\delta\tan(\alpha/2)$. The deflection angle $\phi(z)$, as a function of propagation distance z in the N-prism material or magnetic CRP, is then

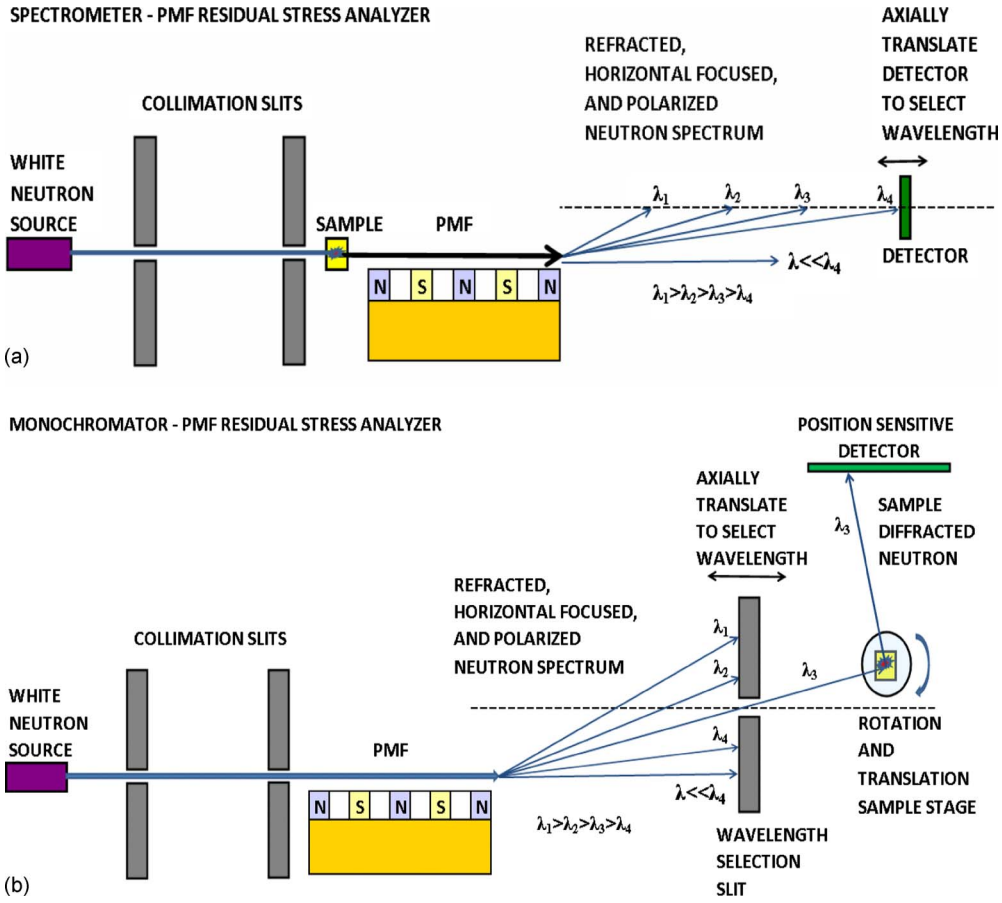

FIG. 8. (Color online) (a) A PMF is used as a spectrometer to perform residual stress analysis with a neutron beam that passes through a sample to the PMF. The PMF line focuses the upward-deflected, spin-up neutrons along a horizontal line parallel to the PMF surface at axial focal distances downstream of the PMF exit that are proportional to the neutron energy. The energy spectrum of the spin-up neutrons from the sample are then measured by an axial-translatable detector (b) A PMF acts as a monochromator to produce a narrow bandwidth of spin-up, polarized (aligned) neutrons that illuminate a sample, which then diffracts these neutrons to a fixed, position-sensitive detector.

$\phi(z)=2N(z/l_1)\Delta\theta$, and the deflection angle axial gradient $d\phi/dz$ is

$$\frac{d\phi}{dz}=\frac{2N\delta}{l_1}\tan(\alpha/2). \tag{22}$$

In a material CRP both neutron spin states are equally deflected in the same upward direction away from the prism base. From Eqs. (21) and (22) the deflection angle axial gradient $d\phi/dz$ is

$$\frac{d\phi}{dz}=\left(6.1\sum_{j=1}^{Q}\rho_j b_j\right)\frac{N\lambda^2}{l_1\pi}\tan(\alpha/2). \tag{23}$$

The ratio r_{mat} of the neutron deflection angle gradient at the exit of a N-period PMF [Eq. (11)], divided by that of a material N-prism CRP of the same length l_1 [Eq. (23)] is

$$r_{\mathrm{mat}}=\frac{1.07\times10^{-6}B_0}{\sum_{j=1}^{Q}\rho_j b_j}\cdot\frac{\exp\left(-2\pi\frac{y_0}{p}\right)}{\tan(\alpha/2)}. \tag{24}$$

In a material CRP, the absorption aperture "depth" H_a is defined as the vertical distance from the apex of any one of the individual CRP prisms to a lower horizontal line trajectory in which the transmitted neutron intensity has decreased by a factor e^{-2} relative to the neutron intensity passing just above the N prism apexes, where

$$H_a=\frac{1}{N\mu\tan(\alpha/2)}. \tag{25}$$

For example, at wavelength $\lambda=1.8$ Å the linear attenuation for aluminum is $\mu=0.1$ cm^{-1}, and an aluminum CRP with $N=87$ prisms, each with apex angle $\alpha=60°$, has an absorption aperture depth of $H_a=2.0$ mm. Unlike material CRPs, which have strong attenuation from neutron scatter and absorption, the PMF transmits neutrons without such attenuation.

The PMF is now compared to the magnetic CRP. The magnetic field intensity in the prism-shaped magnetic field should be uniform in the magnetic CRP. The pole pieces can be permanent magnets or soft iron magnetized by an electromagnet, and in either case, a magnetic return circuit is employed to increase the magnetic field amplitude in the gaps. To reduce fringing magnetic fields that cause aberration, the ratio of the pole gap distance divided by the pole surface area should be much less than one. In a magnetic prism the upper energy state, spin-up neutrons are deflected upwards away from the prism base and the spin-down neutrons downwards.

The deflection angle axial gradient $d\phi/dz$ for spin-up neutrons (+) and spin-down neutrons (−) in the magnetic CRP is

$$\frac{d\phi}{dz} = \pm 2.3 \times 10^{-6} B_0 \frac{N\lambda^2}{l_1 \pi} \tan(\alpha/2). \quad (26)$$

The ratio r_{mag} of the neutron deflection angle gradient at the exit of a N-period PMF [Eq. (11)], divided by that of the magnetic N-prism CRP of the same length l_1 [Eq. (26)] is

$$r_{\mathrm{mag}} = \frac{2.84}{\tan(\alpha/2)} \exp\left(-2\pi \frac{y_0}{p}\right). \quad (27)$$

If the magnetic prism apex angles are $\alpha = \pi/3$, and the neutron enters the PMF below the critical height $y_0 < 0.75p/\pi$, then $r_{mag} > 1$, and under these conditions, the PMF provides more deflection than the magnetic CRP. The PMF provides a continuous refraction gradient; whereas, the material and magnetic CRP provide refractive gradients only at the prism interfaces with air or vacuum.

C. Applications of the PMF

One possible application of the PMF is spectral splitting of a white neutron beam for use in residual stress analysis. Consider the PMF spectrometer and monochromator configurations in Fig. 8. In either case the white or wide-band neutron beam is collimated by two narrow, horizontal slits prior to the PMF. The PMF can provide a line-focused beam of aligned (polarized), spin-up neutrons, given a sufficiently high flux neutron source. The horizontal band of spin-up neutrons exits the PMF with their longitudinal magnetic moment component $\mu_{\|}$ aligned antiparallel to the direction of the PMF magnetic field lines at the PMF exit. As the neutrons propagate away from the PMF, the neutrons' $\mu_{\|}$ remain pointed in a fixed direction antiparallel to the direction of their last encountered PMF magnetic lines. The fixed direction of the neutrons' $\mu_{\|}$ at the PMF exit assumes the direction and amplitude of the last encountered PMF magnetic field lines are well defined and dominant over the fringing magnetic fields that extend into the drift space beyond the PMF exit. A very thin, cryocooled superconducting, niobium foil could be placed at the PMF exit to better define its exit magnetic field direction and amplitude, and prevent the undesired outward fringing of PMF magnetic field lines via the Meissner effect.[25]

In the case of the PMF spectrometer shown in Fig. 8(a), the diffracted neutrons from the sample pass through the PMF, which causes the spin-up neutrons to be deflected vertically upward. The spin-down neutrons are downward deflected and strike the PMF. The upward deflected spin-up and polarized neutrons are line-focused at points along a parallel, axial line above the PMF surface at axial distances from the PMF exit that increase proportionally with neutron energy. From the maximum axial distance downstream of the PMF, a horizontal slit detector can be translated axially toward the PMF to measure the energy spectrum of the diffracted neutrons from the sample. Alternatively, without the need for translation, a long fixed, 1D axial position-sensitive detector, which is set y_f to $2y_f$ critical heights ($y_f = 0.75p/\pi$) above the PMF surface plane, could measure the energy spectrum of sample diffracted neutrons.

In the case of a PMF monochromator shown in Fig. 8(b), neutrons pass first through the PMF to produce a narrow-band, spin-up, polarized (aligned) neutron beam, which then propagates to the sample. Upward deflected, spin-up and polarized neutrons are line-focused at points along an axial line y_f to $2y_f$ critical heights above the PMF surface. A horizontal slit in a cadmium sheet is translated axially toward the PMF, which intercepts line-focused neutrons with wavelengths that increase as the scanning slit approaches the PMF. A narrow bandwidth of line-focused, spin-up, and polarized neutrons pass through the slit, and strike the sample position at a particular height that depends on the drift space distance between the scanning slit and sample. Thus, the sample (e.g., machined, cast, or welded part) should be placed on a small translation stage in order to position it at the center of the beam.

If motorized translation stages are used, this results in a system that can be tuned to different wavelengths. The sample rotation stage allows the monochromatized, polarized neutrons to interrogate different crystal planes of the sample lattice. These admitted neutrons are then diffracted by the sample lattice planes to a stationary position-sensitive detector. This detector records the intensity of the sample-diffracted neutrons of wavelength as a function of the diffraction angle, which is measured relative to the line from the PMF exit through the wavelength-selection slit to the sample.

In the two above embodiments of a PMF residual stress instrument, the diffracted neutron intensity as a function of angle and wavelength can be compared with a "calibration" unstressed sample. The sample can then be subjected to compression, torsion, tension, heat, etc., in order to measure residual stress as a function of applied environment, and thus provide structural information and feedback.

Finally, a cylindrical PMF comprised of an axial stack of N annular (washer) magnets, radial magnetized and alternating in polarity, separated by identical aluminum washers, can provide an azimuthally symmetric, periodic radial **B** field throughout its center bore. The cylindrical PMF can thus act as a compound refractive lens to focus the higher energy state, spin-up neutrons and defocus the lower energy, spin-down neutrons in a sufficiently collimated, cylindrical beam with applications as a condenser and/or objective lens in a neutron microscope. The annular magnets are comprised of joined, arc-shaped NdFeB magnets, each arc separately magnetized in the radial direction. The spacer can be designed to encase and bind the mutually repulsive arc magnets, and set the axial spacing between two adjacent annular magnets of opposite radial polarity, which form a period. As an approximation, the planar PMF equations (e.g. focal length) can apply to its cylindrical version with an identical number N of periods p, axial magnet Δz_m and spacer Δz_s widths, and bore surface magnetic field amplitude B_0, if the annular magnet inner (bore) radius r_b is equal to the planar PMF critical height, where $r_b = y_f = 0.75\, p/\pi$. An annular magnet, comprised of eight 45 degree sectors, and with 1.59 mm axial

width, 1.59 mm inner radius, 12.70 mm outer radius, with about $B_0=0.35$ *T* measured on its inner surface, was fabricated for us by J. Stupak of Oersted Technology.[26]

We acknowledge the technical assistance of D. J. Arya. This work was supported in part by U.S. National Institutes of Health and U.S. Department of Energy (Grant Nos. 1 R43 CA115248-01A1 and DE-FG02-03ER83862).

[1] D. J. Hughes, *Neutron Optics* (Interscience, New York, 1954).
[2] W. Just, C. S. Schneider, R. Ciszewski, and C. G. Shull, Phys. Rev. B **7**, 4142 (1973).
[3] A. I. Frank, Usp. Fiziol. Nauk **151**, 229 (1987).
[4] A. I. Frank, Atomnaya Energiya **66**, 93 (1989).
[5] H. M. Shimizu, Appl. Phys. A: Mater. Sci. Process. **74**, s326 (2002).
[6] T. Shinohara, K. Hirota, T. Adachi, K. Ikeda, H. M. Shimizu, J. Suzuki, and T. Oku, Physica B **385**, 1232 (2006).
[7] K. C. Littrell, S. G. E. te Velthuis, G. P. Felcher, S. Park, B. J. Kirby, and M. R. Fitzsimmons, Rev. Sci. Instrum. **78**, 035101 (2007).
[8] E. M. Forgan and R. Cubitt, Neutron News **9**, 25 (1998).
[9] M. R. Eskildsen, P. L. Gammel, E. D. Isaacs, C. Detlefs, K. Mortensen, and D. J. Bishop, Nature (London) **391**, 563 (1998).
[10] S. M. Choi, J. G. Barker, C. J. Glinka, Y. T. Cheng, and P. L. Gammel, J. Appl. Crystallogr. **33**, 793 (2000).
[11] J. T. Cremer, M. A. Piestrup, C. K. Gary, R. H. Pantell, and C. J. Glinka, Appl. Phys. Lett. **85**, 494 (2004).
[12] H. Park, J. T. Cremer, M. A. Piestrup, C. K. Gary, R. P. Hjelm, W. C. L. J. Sellyey, R. H. Pantell, and X. Wu, Nucl. Instrum. Methods Phys. Res. B **251**, 507 (2006).
[13] J. T. Cremer, H. Park, M. A. Piestrup, C. K. Gary, R. H. Pantell, R. G. Flocchini, H. P. Egbert, M. D. Kloh, and R. B. Walker, Appl. Phys. Lett. **90**, 141113 (2007).
[14] V. F. Sears, *Neutron Optics* (Oxford University Press, New York, 1989).
[15] W. G. Williams, *Polarized Neutrons* (Clarendon, Oxford, 1988).
[16] T. J. L. Jones and W. G. Williams, J. Phys. E **13**, 227 (1980).
[17] A. G. Siegman, *An Introduction to Lasers and Masers* (McGraw Hill, New York, 1971).
[18] C. Kittel, *Introduction to Solid State Physics* (Wiley, New York, 2005).
[19] J. W. Akitt and B. E. Mann, *NMR and Chemistry: An Introduction to Modern NMR Spectroscopy* (Stanley Thornes, Cheltenham, UK, 2000).
[20] R. L. Liboff, *Introduction to Quantum Mechanics* (Addison-Wesley, Reading, MA, 2003).
[21] W. N. Cottingham and D. A. Greenwood, *An Introduction to Nuclear Physics* (Cambridge, Cambridge, UK, 2001).
[22] D. R. Stump and G. L. Pollack, Eur. J. Phys. **19**, 59 (1998).
[23] FujiFilm Medical Systems USA, Inc., Stamford, CT.
[24] B. T. M. Willis and C. J. Carlile, *Experimental Neutron Scattering* (Oxford University Press, New York, 2009).
[25] R. O. Tatchyn, P. L. Csonka, and J. T. Cremer, U.S. Patent No. 4,977,384 (1990).
[26] Oersted Technology, Troutdale, OR, www.oersted.com.